

Ion Selectivity of α -Hemolysin with a β -Cyclodextrin Adapter. I. Single Ion Potential of Mean Force and Diffusion Coefficient

Yun Luo,[†] Bernhard Egwolf,[†] D. Eric Walters,[‡] and Benoît Roux^{*,†}

Department of Biochemistry and Molecular Biology, The University of Chicago, Chicago, Illinois, and Department of Biochemistry and Molecular Biology, Rosalind Franklin University of Medicine and Science, North Chicago, Illinois

Received: July 17, 2009; Revised Manuscript Received: November 20, 2009

The α -hemolysin (α HL) is a self-assembling exotoxin that binds to the membrane of a susceptible host cell and causes its death. Experimental studies show that electrically neutral β -cyclodextrin (β CD) can insert into the α HL channel and significantly increase its anion selectivity. To understand how β CD can affect ion selectivity, molecular dynamics simulations and potential of mean force (PMF) calculations are carried out for different α HL channels with and without the β CD adapter. A multiscale approach based on the generalized solvent boundary potential is used to reduce the size of the simulated system. The PMF profiles reveal that β CD has no anion selectivity by itself but can increase the Cl^- selectivity of the α HL channel when lodged into the pore lumen. Analysis shows that β CD causes a partial desolvation of ions and affects the orientation of nearby charged residues. The ion selectivity appears to result from increased electrostatic interaction between the ion and the channel due to a reduction in dielectric shielding by the solvent. These observations suggest a reasonable explanation of the ion selectivity and provide important information for further ion channel modification.

Introduction

α -Hemolysin (α HL) secreted by the bacterium *Staphylococcus aureus* is an exotoxin involved in a number of human diseases.^{1–3} It can self-assemble on lipid bilayers of a susceptible host cell membrane to form a wide heptameric pore.⁴ Uncontrolled permeation of water, ions, and small organic molecules through this wide transmembrane pore can then lead to the death of the host cell.⁵ Being a particularly robust structure, α HL has many potential applications in biotechnology, such as single-molecule detection,^{6–10} single DNA sequencing,¹¹ nanochemistry,^{12,13} nanoelectro-osmotic transportation,¹⁴ and modulation of ion selectivity.¹⁵ Important aspects of α HL as a promising scaffold for synthetic ion channels are as follows: (1) it can bind to various biological or synthetic lipid bilayers readily and spontaneously; (2) once bound to the membrane, it is stable over a wide range of pH and temperature; (3) it can be modulated in many ways to adjust ion selectivity. Experimental studies show that the wild-type α HL displays a weak anionic selectivity and this selectivity can be increased by mutation of residues lining the lumen of the channel,¹⁶ and by noncovalent^{7,15–17} or covalent linkage¹⁸ of a cyclic polysaccharide (β -cyclodextrin) in the lumen of the pore. For example, the $(\text{M113N})_7$ mutant and $(\text{M113F})_7$ mutant α HL channels have been reported to be able to bind the β -cyclodextrin (β CD) noncovalently for 10^4 times longer than the wild-type α HL^{17,16} and become highly chloride ion selective.¹⁵ However, β CD is an electrically neutral molecule and the underlying mechanism for the high chloride selectivity is unclear. To facilitate the chemical ion channel design, it is essential to understand how β CD improves the anion selectivity of the channel. Because

ion selectivity is often dominated by relative free energy differences, molecular dynamics potential of mean force (PMF) calculation is a powerful approach to deepen our understanding of the ion selectivity mechanisms at the atomic level. Here, molecular dynamics (MD) free energy simulations are carried out for different α HL channels with and without β CD adapted inside. To reduce the size of the simulated system, a multiscale approach based on the generalized solvent boundary potential (GSBP) is used whereby the local system is simulated with atomic detail and the effects of the surroundings are approximated with continuum electrostatics.¹⁹

The outline of the article is as follows. In the following section, the theoretical background, the system preparation, and details about the simulation are briefly described. Then, the interactions of isolated β CD with ions are calculated, first in vacuum and then in explicit water solvent. The free energy of ion passage through the β CD adapted channel $(\text{M113N})_7 \beta$ CD and $(\text{M113F})_7 \beta$ CD is investigated and compared with the free energy in the isolated channels and wild-type channel. Finally, the main results are summarized in the last section.

Methods

Atomic Model and GSBP Method. The CHARMM PARAM27²⁰ force field was used for the protein, and the TIP3P was used for the water molecules.²¹ The generalized AMBER force field (GAFF)²² was used to model β CD. The topology and parameters of β CD for CHARMM were generated with ANTECHAMBER 1.27²³ and with AM1-BCC²⁴ partial charges (provided in the Supporting Information, Tables S1 and S2). The electrostatic potential surface of β CD was produced using Molecular Operating Environment, version 2007.09 (Chemical Computing Group, Montreal), and AM1-BCC partial atomic charges.²⁴ A Gaussian surface was generated, and the potential was calculated using the Poisson–Boltzmann (PB) equation.²⁵ The parameters for K^+ and Cl^- were taken from ref 26. Five

* To whom correspondence should be addressed. E-mail: roux@uchicago.edu.

[†] The University of Chicago.

[‡] Rosalind Franklin University of Medicine and Science.

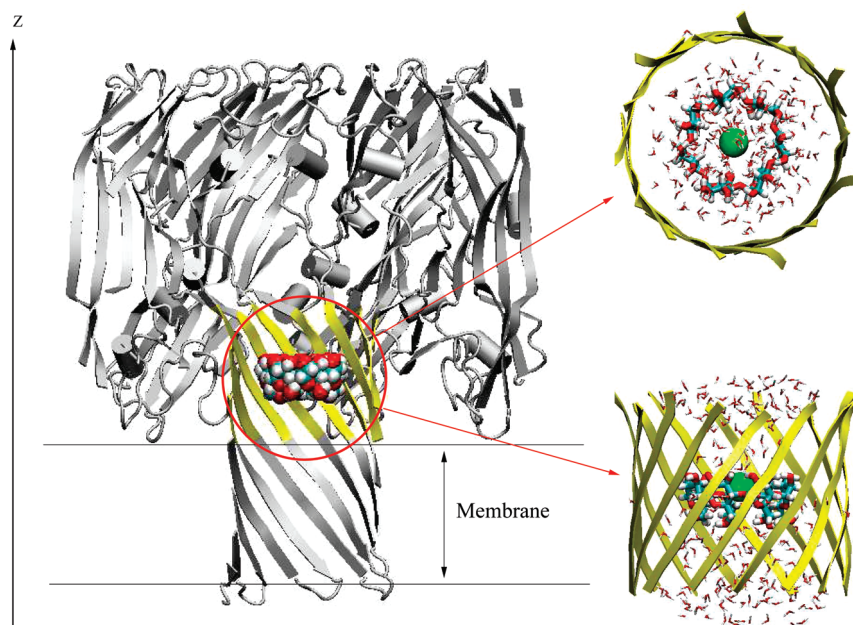


Figure 1. Molecular graphics view of the GSBP simulation system for the $(M113N)_7$ channel with a β CD adapter inside. The full protein is shown in cartoon style (gray), while the inner GSBP simulation region is highlighted in yellow. The channel axis is along the z -axis. The implicit membrane is centered at $z = 0 \text{ \AA}$ with a thickness of 25 \AA . The reduced system for GSBP is zoomed in and shown in top view and side view. The residues in the inner region, yellow ribbons; β CD, VDW model in whole channel and licorice model in zoomed-in figure; Cl^- , green sphere; TIP3 water, stick in atom type colors.

channel systems were generated using CHARMM^{27,28} on the basis of available X-ray structures. They are wild-type (wt) α HL,²⁹ $(M113N)_7$, $(M113F)_7$, $(M113N)_7\beta$ CD, and $(M113F)_7\beta$ CD (Montoya and Gouaux, unpublished). However, there is one side chain missing in the $(M113F)_7$ crystal structure (Lys110 → Gly110) and two side chains missing in the $(M113N)_7$ crystal structure (Tyr148 → Ala148, Leu1288 → Gly1288). We modified the $(M113F)_7$ structure by adding back the charged Lys110, while keeping the $(M113N)_7$ crystal structure unchanged. Hydrogen atoms were added using the HBUILD facility in CHARMM. The protonation state of the channels was chosen as in Noskov et al.³⁰ In the simulations, the channel structures are oriented with their pore along the z -axis. The negative z -axis corresponds to the intracellular side (*trans* side), and the positive z -axis corresponds to the extracellular side (*cis* side). The center of the implicit membrane is located at $z = 0 \text{ \AA}$, extending in the x and y directions with a thickness of 25 \AA (Figure 1). In the X-ray structures, the seven glucose 6-OH groups of β CD point toward the *trans* side in the $(M113N)_7\beta$ CD channel but toward the *cis* side in the $(M113F)_7\beta$ CD channel. The center of mass of β CD is located approximately on the z -axis around 25 \AA in the $(M113N)_7\beta$ CD system and at 26 \AA in the $(M113F)_7\beta$ CD system. The pore radius profiles of the three X-ray structures of isolated channels are calculated using CHARMM (Figure 2).

The GSBP method implemented into the PBEQ module^{31–33} of the CHARMM program was used to simulate a reduced atomic model of α HL. The multiscale approach based on the GSBP is similar to the semimicroscopic approach in existing literature.^{34–37} The theoretical foundation about the GSBP method can be found in ref 19. In our simulation, a spherical inner region was centered at $(0.0, 0.0, 30.0)$, with a radius of 20 \AA . The inner region was extended by 3 \AA to define a smooth spherical dielectric cavity of 23 \AA . Protein atoms near the edge of the boundary were fixed during the simulation. In the inner region (see Figure 1 for top view and side view), the protein, the cyclodextrin, and the solvent molecules were simulated

explicitly with all-atom MD simulations. In the outer region, the remaining protein atoms and solvent were treated implicitly. The influence of the surrounding outer region on the atoms of the inner region is represented in terms of a solvent-shielded static field ϕ_{sf} and a solvent-induced reaction field ϕ_{rf} . The reaction field due to changes in charge distribution in the dynamic inner region is expressed in terms of a basis set expansion of the inner region charge density. The solvent-shielded static field from the outer region $\phi_{sf}^{(0)}$ and the reaction field matrix M_{mn}^* , representing the couplings between the generalized multipoles were calculated once and recalled during the later simulations. Dielectric constants were assigned values of 80 for solvent and 2 for both protein and membrane. The finite-difference PB calculation was solved with periodic boundary conditions in the xy -plane. The KCl concentration was assumed to be 150 mM in the bulk solvent. The reaction field matrix and static field were calculated using a 111^3 coarse grid with a grid spacing of 3.0 \AA , followed by a 161^3 fine grid centered at the center of mass of β CD with a grid spacing of 0.5 \AA . The reaction field matrix was built using 25 basis functions of five multipoles without sorting. After defining the inner region and calculating the static field and reaction field matrix, the inner region system was hydrated with explicit TIP3P water molecules. We used 20 cycles of 10 000 steps of Monte Carlo (MC) followed by 10 000 steps of Langevin dynamics. The MC consists of rigid body translation, rotation, and GCMC (grand canonical Monte Carlo) moves with equal probability. A friction coefficient of 5 ps^{-1} was assigned to all nonhydrogen atoms for the Langevin dynamics.

The Potential of Mean Force. The 1D-PMF $W(z)$ was calculated using umbrella sampling,³⁸ in which a set of equally spaced simulations were biased by the quadratic potential $w_i(z) = (1/2)k_i(z - z_i)^2$ to restrain the ion near specific positions z_i along the z -axis; 61 independent windows, separated by 0.5 \AA increments in the z direction from 15 to 45 \AA , were simulated with Langevin dynamics. A force constant of $5 \text{ kcal/mol}/\text{\AA}^2$ was used for the harmonic potential to ensure overlap of neighboring

windows. A time step of 2 fs was used for all simulations, and a friction constant of 5 ps⁻¹ was applied to all nonhydrogen atoms. Each window simulation started from the configuration equilibrated during 20 ps with the ion near the constraint position. 500 ps of trajectory was generated for each window. The results were unbiased using the weighted histogram analysis method (WHAM),³⁹ with a bin size of 0.05 Å and a stringent tolerance of 0.0001 kcal/mol on every point in the PMF.

For calculating the PMF of one ion passage through βCD in explicit solvent, the βCD is located in the center of a cylinder of TIP3P water molecules. The cylinder of solvent contains 404 TIP3P molecules and is about 62 Å in length and 7.6 Å in radius. Periodic boundary conditions were used for the cylinder system (tetragonal box 31 × 31 × 62 Å³ with a cutoff distance of 15 Å). The parameters for umbrella sampling are the same as those in the channel system described above.

PB Computations. Continuum electrostatic calculations were carried out by moving one ion along the *z*-axis by 1.0 Å increments through the whole channel. The aqueous solution (including the water-filled cavity at the center of the channel) was represented as a uniform continuum media with a dielectric constant of 80. The channel with all explicit atoms was embedded into a low dielectric planar slab simulating the membrane, represented as a uniform slab of 25 Å thickness with a dielectric constant of 2.⁴⁰ The crystal structures were used. The dielectric constant of the protein interior was assumed to be 2. All calculations were performed using the PBEQ module,^{31–33} implemented in CHARMM.^{27,28} The atomic charges were taken from the all-atom PARAM27 force field of the CHARMM program, and the atomic radii used to define the protein–solvent dielectric boundary were taken from previous free energy simulation studies with explicit water molecules.³¹ Each PB calculation was performed in two steps with a cubic grid of 240³ points, starting with a grid spacing of 1.0 Å, followed by a focusing around the main region with a grid spacing of 0.5 Å.

Position-Dependent Diffusion Coefficient of Ions. The position-dependent diffusion coefficients of K⁺ and Cl⁻ inside the βCD were calculated from the umbrella sampling MD trajectories using the GSBP reduced (M113N)₇ βCD system. The details about the simulations are the same as described in the PMF calculations, except that the Langevin dynamics was turned off within a radius of 12 Å from the center by setting the parameter RBUF = 12. The theoretical formulation used here was previously elaborated by Hummer,⁴¹ based on an early development by Woolf and Roux.⁴² Briefly, the position-dependent diffusion coefficient $D(z)$ along the *z*-axis aligned with the pore is expressed as,

$$D(z_i) = \frac{\langle \delta z^2 \rangle_{(i)}}{\tau_i} \quad (1)$$

where τ_i is the correlation time extracted from the biased simulation with the *i*th window potential,

$$\tau_i = \int_0^\infty dt \frac{\langle \delta z(t) \delta z(0) \rangle_{(i)}}{\langle \delta z^2 \rangle_{(i)}} \quad (2)$$

and $z(t)$ is the position of the ion along the *z*-axis, $\delta z(t) = z(t) - \langle z \rangle_{(i)}$. The diffusion coefficients in bulk are computed from additional MD simulations in which a K⁺ or Cl⁻ was placed in a droplet of about 600 explicit TIP3P water molecules, contained

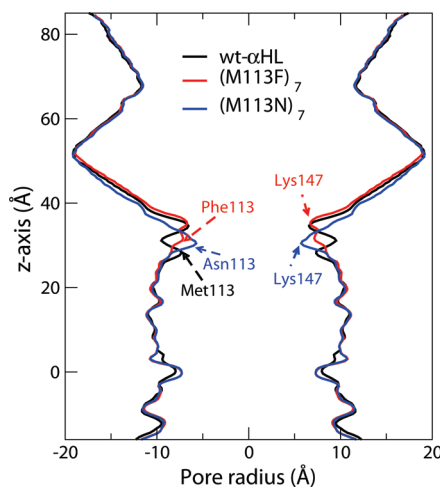


Figure 2. Pore radius profiles along the channel axis calculated using the CHARMM program. wt-αHL is in black, (M113F)₇ is in red and (M113N)₇ is in blue. The positions of residue 113 and 147 in each channel are pointed out with the same color as the channel profile.

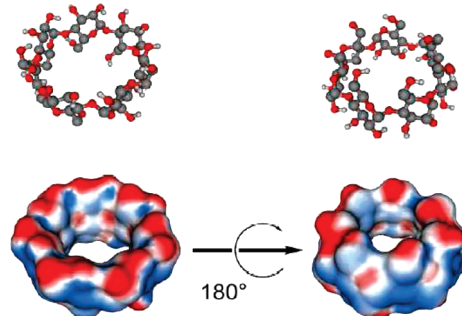


Figure 3. β-cyclodextrin is shown as ball-and-stick models and as Connolly surfaces onto which electrostatic potential is mapped (blue = positive, red = negative). Partial atomic charges and force field parameters were calculated using the general Amber force field/AM1/BCC method.²²

by the reactive spherical solvent boundary potential (SSBP).²⁶ The ion was restrained near the center of the droplet by a harmonic potential. The diffusion coefficients in bulk calculated using the same equations (eqs 1 and 2) are 0.33 Å²/ps for both K⁺ and Cl⁻, which is in agreement with a previous MD study.⁴³

Results and Discussion

Ion Selectivity of βCD. Figure 3 shows the electrostatic potential surface of βCD calculated in a vacuum. The potential is slightly more positive through the lumen of the cyclodextrin (blue and red surfaces indicate a positive and negative potential, respectively). The ion selectivity of βCD alone was first examined by moving one ion through βCD in a vacuum. The results are shown in Figure 4A. The vacuum interaction energy profiles of K⁺ and Cl⁻ have symmetric and opposite interactions, mainly due to the charge distribution of the βCD. In a vacuum, the passage of Cl⁻ is opposed by a larger energy barrier than K⁺. As shown in Figure 4B and D, the large energy barriers observed in a vacuum are considerably reduced by the influence of solvation. In Figure 4B, the electrostatic free energy of a single ion passing through βCD was calculated using continuum electrostatics Poisson–Boltzmann (PB). In Figure 4D, the corresponding free energy profiles were calculated using umbrella sampling MD simulations with explicit solvent molecules. The latter reveal relatively complex interactions, due in part to solvation and desolvation effects of the ions as they pass

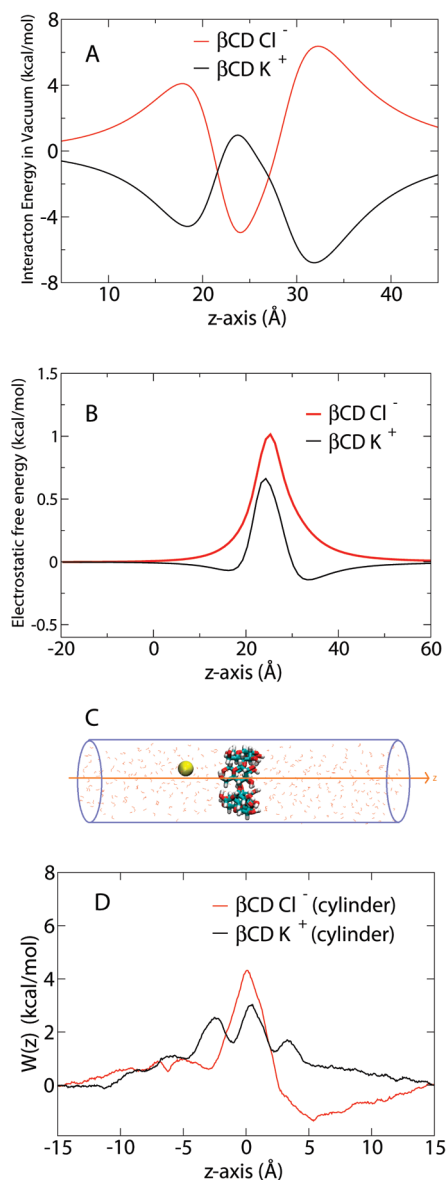


Figure 4. (A) Interaction of K^+ and Cl^- ions with β CD in a vacuum. β CD is located at $z = 25 \text{ \AA}$. The ion is moving from 5 to 45 \AA through β CD along the z -axis. (B) The electrostatic free energy profiles of ion passage through β CD, obtained from PB calculations. β CD is located at $z = 25 \text{ \AA}$. (C) The cartoon of single ion passage through β CD in the cylinder of explicit water solvent. β CD, licorice in atom type colors; K^+ as a yellow sphere; TIP3 water in red stick. (D) 1D-PMF of K^+ and Cl^- passage through β CD in the cylinder of explicit water solvent.

through the small aperture of β CD. Nevertheless, while there are quantitative differences, Figure 4B and D shows that β CD, by itself, is not selective for Cl^- over K^+ when solvation effects are taken into account.

Ion Selectivity of Isolated Ion Channel and β CD Adapted Ion Channel. The influence of the β CD and the pore architecture on the ion transfer is investigated for five α HL channel systems: wt- α HL, ($M113N_7$), ($M113F_7$), ($M113N_7$) β CD, and ($M113F_7$) β CD. For each system, the PB calculations and the PMF calculations were carried out as described in the Methods section. The channel pore radius of the crystal structures versus position along the channel axis (Figure 2) shows that there are two constriction regions inside the channels. The first one is at the top of the β -barrel (near $z = 30\text{--}35 \text{ \AA}$), with a total charge of +7e (7 Glu and 14 Lys residues). The second constriction region is at the transmembrane domain (near $z = 0 \text{ \AA}$), with a

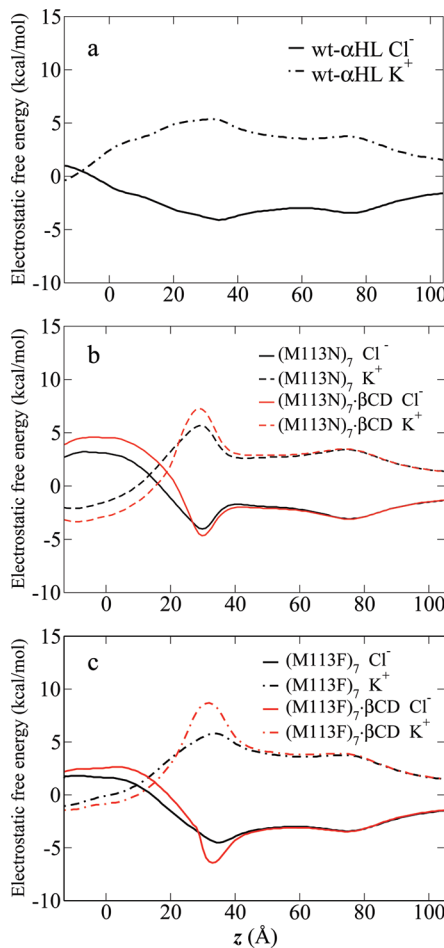


Figure 5. Electrostatic free energy profiles of ion passage through five channels, obtained from PB calculations. The solid lines are Cl^- profiles, and the dashed lines are K^+ profiles.

total charge of $-7e$ (7 Lys and 14 Asp residues). The free energy in the PB calculations is dominated by these two regions. Figure 5 shows the electrostatic free energy profiles obtained from PB calculations by moving one ion along the z -axis through the five channels. These profiles show that the free energy minima for Cl^- (solid lines) and maxima for K^+ (dashed lines) are located from $z \sim 30$ to 35 \AA . In the transmembrane region (z between -12 and 12 \AA), the free energy of Cl^- goes up and that of K^+ goes down. These electrostatic free energy profiles correspond to the common feature of the α HL structure.

The structural difference among three channels, wt- α HL, ($M113N_7$), and ($M113F_7$), is only at residue 113, which is located near $z = 29 \text{ \AA}$. The large change in the electrostatic free energy profiles with the neutral mutation is actually caused by the different orientation of Asp128 and Lys131 side chains at the bottom of the crystal structures. This can be confirmed by reconstructing the ($M113N_7$) and ($M113F_7$) mutants from the wt- α HL X-ray structure while keeping the configuration of the other side chains unchanged. The PB calculations on these model structures, shown in Figure 6, confirm that residue 113 does not give rise to a long-range effect in the transmembrane region. Comparing the energy profiles in the β CD adapted channels (red lines) with the isolated channel (black lines), Figure 5b and c both show that the electrostatic free energy barrier between Cl^- and K^+ is higher in the β CD adapted channels than in the isolated channel.

Figure 7 shows the PMF of Cl^- (red line) and K^+ (blue line) in the GSBP inner region of the five channels. The PMF profiles

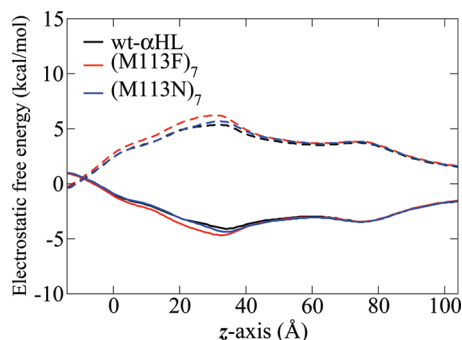


Figure 6. Electrostatic free energy profiles obtained from PB calculations. The $(M113N)_7$ and $(M113F)_7$ mutants are reconstructed from the wt- α HL X-ray structure, with the configuration of the other side chains unchanged. The solid lines are Cl^- profiles, and the dashed lines are K^+ profiles.

of the isolated channels (Figure 7a–c) are relatively smooth and symmetric, similar to the electrostatic free energy obtained from PB calculations (dashed lines). These profiles suggest that the ion selectivity in the isolated channels is dominated by electrostatic interaction between the ion and the channel. The largest free energy differences between the Cl^- and K^+ are found near $z \sim 35$ Å in wt- α HL and the $(M113F)_7$ (Figure 7a and c) and near $z \sim 31$ Å in the $(M113N)_7$ mutant (Figure 7b). Those positions correspond to the narrowest region in each channel,

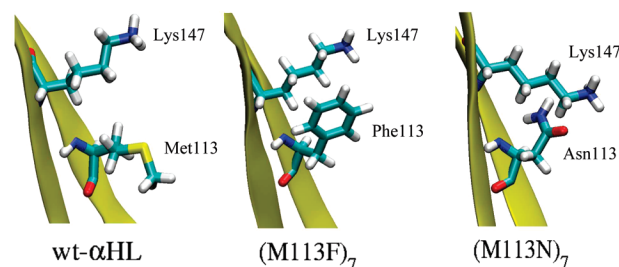


Figure 8. Snapshots of a partial segment of channels showing the orientation of Lys147 and the residue at position 113 in three crystal structures. The $(M113F)_7$ has Lys147 in the same orientation as the wt- α HL, while in the $(M113N)_7$ Lys147 is pointing slightly downward.

where seven Lys147 residues are located (see the pore radius profile in Figure 2). The position of the narrowest region in the $(M113N)_7$ is lower along the z -axis than the other channels because of the different orientations of Lys147 residues. The snapshots of partial X-ray structures in Figure 8 show that Lys147 residues are pointing upward in both wild-type and the $(M113F)_7$, while they are pointing slightly downward in the $(M113N)_7$. The Lys147 has a considerable impact on the PMF because the seven positively charged side chains form a narrow ring, giving rise to a very strong electrostatic field in this region of the pore.

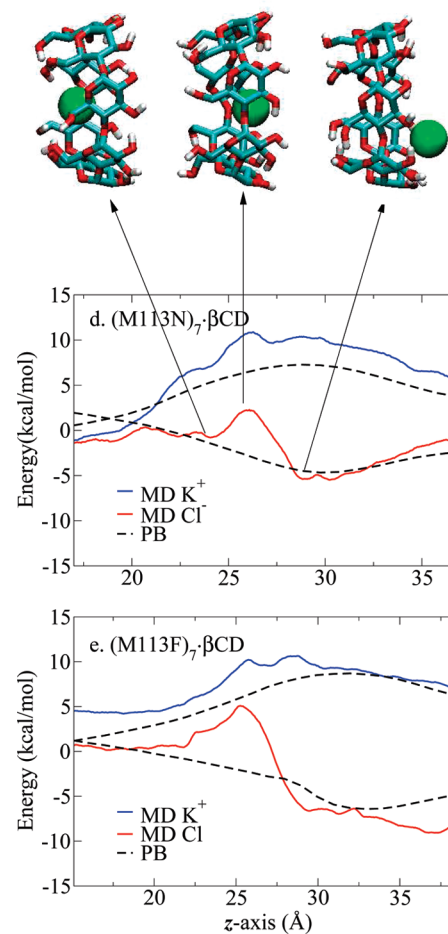
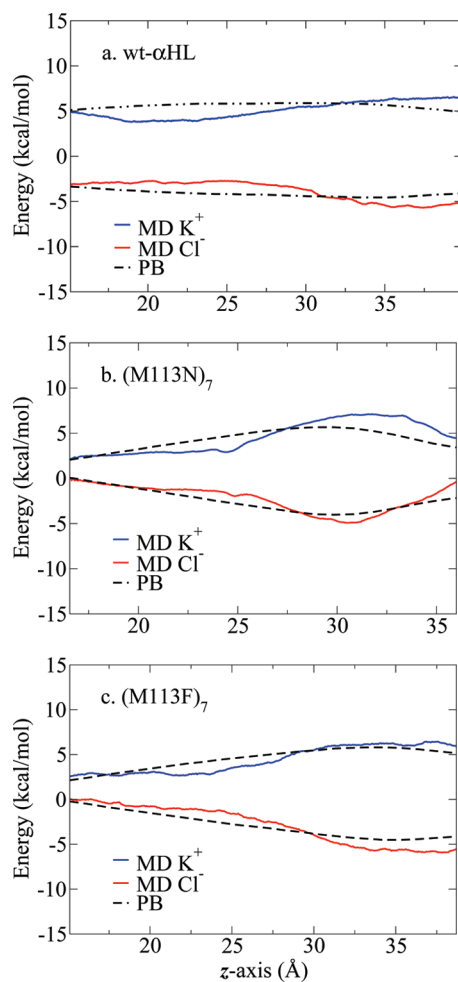


Figure 7. 1D-PMF profiles of ion passage through five channels. In PMF profiles, the red line is the Cl^- profile, the blue line is the K^+ profile, and the dashed line is the electrostatic free energy profile. Three snapshots show the Cl^- position corresponding to the z coordinates in the PMF profile. β CD is in licorice with atom type colors; Cl^- as a green sphere; protein and TIP3 water molecules are not shown here.

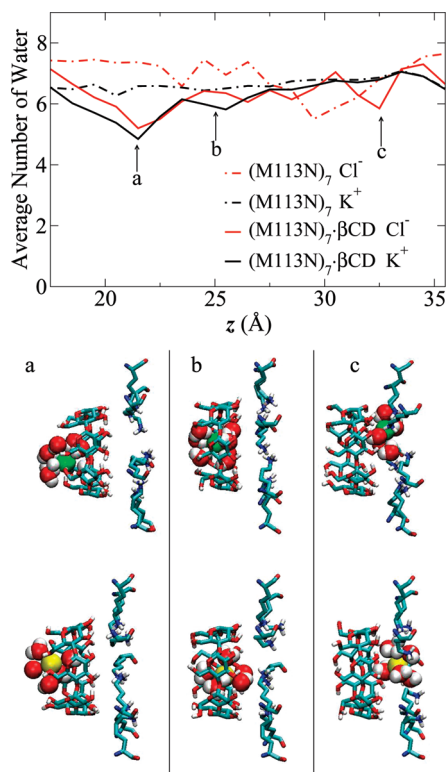


Figure 9. Average number of water molecules in the first solvation shell of ion inside $(M113N)_7$ and $(M113N)_7$ β CD channels. A radius cutoff of 3.7 Å is used for Cl^- (red lines) and 3.5 Å for K^+ (black lines). Snapshots show the typical ion and water configurations inside the $(M113N)_7$ β CD channel at an ion position of (a) $z \sim 21$ Å, (b) $z \sim 25$ Å, and (c) $z \sim 33$ Å. The three positions are also pointed out in the figure. Cl^- in green VDW sphere; K^+ in yellow VDW sphere; TIP3P water in VDW sphere with atom type colors; both β CD and Lys147 residues are shown in licorice style with atom type colors. Only water molecules within the first hydration shell are shown here; other residues and water molecules are omitted for clarity.

Figure 7d and e show the PMF of Cl^- and K^+ in β CD adapted channels. These PMF profiles are clearly distinct from the one without β CD (Figure 7b and c). The Cl^- PMF in the $(M113N)_7$ β CD channel features three distinct areas (Figure 7d). As illustrated in the inserted snapshots, the PMF is unfavorable when Cl^- goes through the β CD. The local energy barrier, similar to Figure 4D, reaches a maximum near the center of the β CD. Then, the free energy goes down and reaches a minimum when the Cl^- exits the β CD cavity. The K^+ PMF remains unfavorable, displaying no region of appreciable stabilization in the inner region. Similar features are also found in $(M113F)_7$ β CD profiles (Figure 7e).

The Effect of β CD in the Mutant Channels. The PMF profiles show that the β CD can change the free energy of Cl^- and K^+ near the adapter region. Further analysis was performed to elucidate the role of the β CD in the lumen of the pore. First, β CD causes the partial desolvation of both ions. Taking the $(M113N)_7$ β CD system as an example, the average number of water molecules in the first solvation shell of Cl^- (red lines) and K^+ (black lines) are shown in Figure 9. The first solvation shell radii are 3.7 Å for Cl^- and 3.5 Å for K^+ , based on the radial distribution function (RDF) curves (not shown here). Comparing the water profile in $(M113N)_7$ β CD (solid lines) with the one in the isolated channel (dashed lines), about two water molecules are removed when Cl^- or K^+ approaches the small rim of β CD (position a in Figure 9). When the ions are near this position, the primary hydroxyl groups on β CD are able to

rotate freely and interact with both Cl^- or K^+ . The snapshots in Figure 9a show typical configurations of ions with their hydration shell near this position (Cl^- in green, K^+ in yellow). After entering the β CD cavity, both ions stay in the center of the cavity and no special interaction is observed (snapshot b). Hence, the first solvation shell is partially restored in the β CD cavity (position b in Figure 9). When the ions exit the β CD and approach the Lys147 ring, there is a strong electrostatic interaction between the ions and positive amino groups of Lys147 (snapshot c). However, the first solvation shell of K^+ remains intact, while the Cl^- loses one water molecule, as shown in the water profile (position c in Figure 9). This can be explained by the strong electrostatic interaction between Cl^- and Lys147, which disrupts the hydration shell of the anion. The presence of β CD also affects the orientation of the side chain of Lys147. The angle distributions of the Lys147 side chain (Supporting Information, Figure S1) suggests that β CD can restrict the rotation of Lys147 by forming hydrogen bonds between the hydroxyl group on β CD and Lys147 side chain in the $(M113N)_7$ mutant. The $(M113F)_7$ β CD profile (Supporting Information, Figure S1d) also suggests that the partial desolvation of Cl^- caused by β CD increases the electrostatic interaction between Cl^- and the positively charged Lys147 residues.

Position-Dependent Diffusion Coefficient. At this point, our analysis has been exclusively focused on structural and energetic factors associated with ion movement. However, permeation can also be affected by purely dissipative factors, such as the friction or mobility coefficient along the pore.⁴⁴ For instance, the position-dependent diffusion coefficient of ions is a central input parameter in many theoretical descriptions of permeation.^{43,45–47} To determine whether this plays an important role on the anionic selectivity induced by β CD, the diffusion coefficients of K^+ and Cl^- along the pore axis were calculated using biased simulations. The umbrella sampling MD trajectories of $(M113N)_7$ β CD were used. The diffusion coefficient profiles of K^+ and Cl^- as a fraction to bulk values along the channel axis ($15 < z < 35$) are shown in the Supporting Information (Figure S2). The bulk value is $0.33 \text{ \AA}^2/\text{ps}$ for both K^+ and Cl^- , as observed in previous studies of OmpF.^{43,47} The average fraction of bulk diffusion coefficient inside the β CD ($21 < z < 29$) is about 0.115 for both K^+ and Cl^- . There is a reduction by about a factor of 10 in the narrowest part of the pore relative to the bulk. In a continuation of the present study,⁴⁸ the information about the position-dependent diffusion coefficients of K^+ and Cl^- calculated here from all-atom MD simulation with explicit solvent will be incorporated into Brownian dynamics (BD) simulations to generate multi-ion GCMC/BD simulations.⁴⁵ The present results will be important to calibrate the BD simulations, particularly within the narrowest region in the pore through the β CD.

Conclusion

We have performed PMF calculations for five different α HL channels to elucidate the ability of a β CD adapter to increase the anion selectivity of these channels. The free energy profiles suggest that β CD alone has no intrinsic Cl^- selectivity over K^+ , but it can increase the Cl^- selectivity of the α HL mutants when lodged inside the lumen of the pore. A detailed trajectory analysis shows that the β CD causes a partial desolvation of the ions and also affects the orientation of nearby charged residues. The ion selectivity appears to be improved when the ion is less shielded by the solvent, which increases the electrostatic interaction between the ion and the channel. These observations

suggest a reasonable explanation of the ion selectivity and provide important information for further channel modification. For example, the cyclodextrin can be modified by adding positively charged groups to increase anion selectivity or by adding bulky groups to increase the desolvation effect. The modified cyclodextrins can be inserted into the channel, and their effect on ion selectivity can be rapidly evaluated by the computational inexpensive single ion PMF calculation. A large number of known channelopathies require multiple channel modifications to adjust ion selectivity. For example, cystic fibrosis is caused by a defect in a gene coding for an anion channel.³ The present study shows that computational simulations provide an efficient way to predict the ion selectivity, and could further support the experimental exploration of artificial ion channel design.

One important aspect missing from the present study is the influence of multiple ions inside the pore. The anion selectivity displayed by the single ion PMFs with and without β CD seems overestimated. In a wide channel like α HL, multi-ion screening is expected to impact the electrostatic interactions between the pore and the ions. One can expect that the multi-ion PMF will be less dominated by the electrostatic interaction, therefore becoming more sensitive to the geometry of the pore. This part is discussed in the follow-up study.⁴⁸

Acknowledgment. We are very grateful to Eric Gouaux and Michelle Montoya for making available to us the X-ray structure coordinates of the α HL mutants with and without β CD adapted prior to publication. Helpful discussions with Hagan Bayley, Haichen Wu, Haibo Yu, Ed Harder, Xiaoxia Ge, Yuhui Li, Devleena Shivakumar, and Yuqing Deng are gratefully acknowledged. This work was supported by the National Institutes of Health (NIH) through the NIH Roadmap for Medical Research (award number PHS 2 PN2 EY016570B).

Supporting Information Available: Figures showing the effect of the β CD on the orientations of Lys147 residues and diffusion coefficient profiles of K^+ and Cl^- ; Tables showing the topology file of one residue of β CD for CHARMM and the parameter file of β CD for CHARMM. This material is available free of charge via the Internet at <http://pubs.acs.org>.

References and Notes

- (1) Laestadius, A.; Richter-Dahlfors, A.; Aperia, A. *Kidney Int.* **2002**, *62*, 2035–2042.
- (2) Gentschev, I.; Dietrich, G.; Goebel, W. *Trends Microbiol.* **2002**, *10*, 39–45.
- (3) Rowe, S. M.; Miller, S.; Sorscher, E. J. *N. Engl. J. Med.* **2005**, *352*, 1992–2001.
- (4) Gouaux, E. *J. Struct. Biol.* **1998**, *121*, 110–122.
- (5) Aksimentiev, A.; Schulten, K. *Biophys. J.* **2005**, *88*, 3745–3761.
- (6) Bayley, H.; Cremer, P. S. *Nature* **2001**, *413*, 226–230.
- (7) Gu, L.-Q.; Braha, O.; Conlan, S.; Cheley, S.; Bayley, H. *Nature* **1999**, *398*, 686–690.
- (8) Braha, O.; Gu, L. Q.; Zhou, L.; Lu, X.; Cheley, S.; Bayley, H. *Nat. Biotechnol.* **2000**, *18*, 1005–1007.
- (9) Movileanu, L.; Howorka, S.; Braha, O.; Bayley, H. *Nat. Biotechnol.* **2000**, *18*, 1091–1095.
- (10) Wu, H.-C.; Bayley, H. *J. Am. Chem. Soc.* **2008**, *130*, 6813–6819.
- (11) Astier, Y.; Braha, O.; Bayley, H. *J. Am. Chem. Soc.* **2006**, *128*, 1705–1710.
- (12) Luchian, T.; Shin, S.; Bayley, H. *Angew. Chem., Int. Ed. Engl.* **2003**, *42*, 3766–3771.
- (13) Gu, L. Q.; Cheley, S.; Bayley, H. *Science* **2001**, *291*, 636–640.
- (14) Gu, L. Q.; Cheley, S.; Bayley, H. *Proc. Natl. Acad. Sci. U.S.A.* **2003**, *100*, 15498–15503.
- (15) Gu, L.-Q.; Serra, M. D.; Vincent, J. B.; Vigh, G.; Cheley, S.; Braha, O.; Bayley, H. *Proc. Natl. Acad. Sci. U.S.A.* **2000**, *97*, 3959–3964.
- (16) Gu, L.-Q.; Cheley, S.; Bayley, H. *J. Gen. Physiol.* **2001**, *118*, 481–494.
- (17) Gu, L.-Q.; Bayley, H. *Biophys. J.* **2000**, *79*, 1967–1975.
- (18) Wu, H. C.; Astier, Y.; Maglia, G.; Mikhailova, E.; Bayley, H. *J. Am. Chem. Soc.* **2007**, *129*, 16142–16148.
- (19) Im, W.; Berneche, S.; Roux, B. *J. Chem. Phys.* **2001**, *114*, 2924–2937.
- (20) MacKerell, J. A. D.; Banavali, N.; Foloppe, N. *Biopolymers* **2000**, *56*, 257–265.
- (21) Jorgensen, W. L.; Chandrasekhar, J.; Madura, J. D.; Impey, R. W.; Klein, M. L. *J. Chem. Phys.* **1983**, *79*, 926–935.
- (22) Wang, J.; Wolf, R. M.; Caldwell, J. W.; Kollman, P. A.; Case, D. A. *J. Comput. Chem.* **2004**, *25*, 1157–1174.
- (23) Wang, J. M.; Wang, W.; Kollman, P. A.; Case, D. A. *J. Mol. Graphics* **2006**, *25*, 247–260.
- (24) Jakalian, A.; Jack, D. B.; Bayly, C. I. *J. Comput. Chem.* **2002**, *23*, 1623–1641.
- (25) Grant, J. A.; Pickup, B. T.; Nicholls, A. *J. Comput. Chem.* **2001**, *22*, 608–640.
- (26) Beglov, D.; Roux, B. *J. Chem. Phys.* **1994**, *100*, 9050–9063.
- (27) Brooks, B. R.; Bruccoleri, R. E.; Olafson, B. D.; States, D. J.; Swaminathan, S.; Karplus, M. *J. Comput. Chem.* **1983**, *4*, 187–217.
- (28) Brooks, B. R.; et al. *J. Comput. Chem.* **2009**, *30*, 1545–1614.
- (29) Song, L.; Hobaugh, M. R.; Shustak, C.; Cheley, S.; Bayley, H.; Gouaux, J. E. *Science* **1996**, *274*, 1859–1866.
- (30) Noskov, S. Y.; Im, W.; Roux, B. *Biophys. J.* **2004**, *87*, 2299–2309.
- (31) Nina, M.; Beglov, D.; Roux, B. *J. Phys. Chem. B* **1997**, *101*, 5239–5248.
- (32) Im, W.; Beglov, D.; Roux, B. *Comput. Phys. Commun.* **1998**, *111*, 59–75.
- (33) Roux, B. *Biophys. J.* **1997**, *73*, 2980–2989.
- (34) Jordan, P. *IEEE Trans. NanoBioscience* **2005**, *4*, 94–101.
- (35) Dorman, V. L.; Jordan, P. C. *Biophys. J.* **2004**, *86*, 3529–3541.
- (36) Dorman, V. L.; Jordan, P. C. *J. Chem. Phys.* **2003**, *118*, 1333–1340.
- (37) Dorman, V.; Partenskii, M. B.; Jordan, P. C. *Biophys. J.* **1996**, *70*, 121–134.
- (38) Torrie, G. M.; Valleau, J. P. *J. Comput. Chem.* **1997**, *23*, 187–199.
- (39) Kumar, S.; Rosenberg, J. M.; Bouzida, D.; Swendsen, R. H.; Kollman, P. A. *J. Chem. Phys.* **1992**, *13*, 1011–1021.
- (40) White, S. H.; Wiener, M. C. The liquid-crystallographic structure of fluid lipid bilayer membranes. In *Membrane Structure and Dynamics*; Merz, K., Roux, B., Eds.; Birkhäuser: Boston, MA, 1996; pp 127–144.
- (41) Hummer, G. *New J. Phys.* **2005**, *7*, 34.
- (42) Woolf, T. B.; Roux, B. *J. Am. Chem. Soc.* **1994**, *116*, 5916–5926.
- (43) Im, W.; Roux, B. *J. Mol. Biol.* **2002**, *319*, 1177–1197.
- (44) Roux, B.; Allen, T. W.; Berneche, S.; Im, W. *Q. Rev. Biophys.* **2004**, *37*, 15–103.
- (45) Im, W.; Seefeld, S.; Roux, B. *Biophys. J.* **2000**, *79*, 788–801.
- (46) Im, W.; Roux, B. *J. Chem. Phys.* **2001**, *115*, 4850–4861.
- (47) Im, W.; Roux, B. *J. Mol. Biol.* **2002**, *322*, 851–869.
- (48) Egwolff, B.; Luo, Y.; Walters, D. E.; Roux, B. *J. Phys. Chem. B*, accepted for publication.